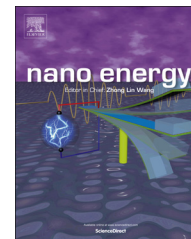




Available online at www.sciencedirect.com

ScienceDirect

journal homepage: www.elsevier.com/locate/nanoenergy



RAPID COMMUNICATION

Magnetocapacitance in magnetic microtubular carbon nanocomposites under external magnetic field



Jiahua Zhu^{a,e}, Minjiao Chen^a, Huige Wei^a, Narendranath Yerra^{a,b},
Neel Haldolaarachchige^c, Zhiping Luo^d, David P. Young^c,
Thomas C. Ho^a, Suying Wei^{a,b,*}, Zhanhu Guo^{a,**}

^aIntegrated Composites Laboratory (ICL), Dan F Smith Department of Chemical Engineering, Lamar University, Beaumont, TX 77710, USA

^bDepartment of Chemistry and Biochemistry, Lamar University, Beaumont, TX 77710, USA

^cDepartment of Physics and Astronomy, Louisiana State University, Baton Rouge, LA 70803, USA

^dDepartment of Chemistry and Physics and Southeastern North Carolina Regional Microanalytical and Imaging Consortium, Fayetteville State University, Fayetteville, NC 28301, USA

^eDepartment of Chemical and Biomolecular Engineering, The University of Akron, Akron, OH 44325, USA

Received 22 January 2014; received in revised form 4 April 2014; accepted 8 April 2014

Available online 18 April 2014

KEYWORDS

Magnetocapacitance;
Magnetoresistance;
Magnetohydrodynamics;
Carbon nanocomposites;
Magnetic field;
Electrochemistry

Abstract

A small external magnetic field of 0.072 T was reported to significantly influence the specific capacitances of the supercapacitor with magnetic carbon - metal (iron, cobalt or nickel) oxides microtubular nanocomposite fabrics as flexible electrodes. The decorated metal oxide species and annealing method (microwave-assisted vs. conventional tubular annealing) were discovered to play important roles in the increase or decrease of the capacitance. All the electrodes demonstrated excellent cycling retention performances, for example, upto ~350% for nickel oxide doped carbon nanocomposite electrodes. The corresponding mechanism for the magnetic field influence on the capacitance has been interpreted in term of a synergistic effect of three internal resistances, solution resistance in electrolyte solution, charge transfer resistance at electrode/electrolyte interface and leakage resistance in electric double layer region. The applied magnetic field is able to change the solution resistance due to the

*Corresponding author at: Department of Chemistry and Biochemistry, Lamar University, Beaumont, TX 77710, USA. Tel.: +1 409 880 7976.

**Corresponding author. Tel.: +1 409 880 7654.

E-mail addresses: suying.wei@lamar.edu (S. Wei), zhanhu.guo@lamar.edu (Z. Guo).

magneto-hydrodynamic phenomena as well as the electrode resistance (directly corresponds to charge transfer resistance) by the magneto-resistance (MR) behavior.

© 2014 Elsevier Ltd. All rights reserved.

Introduction

The ever increasing demand for high-power energy resources in hybrid electric vehicles has triggered great interest in the development of supercapacitors due to their high power supply, long term stability and environmental benign nature [1]. The commercial supercapacitors usually suffer from low energy density and poor cycling stability due to the low electrical conductivity of electrode material and structural damage at electrode surface owing to the insufficient tolerance of volume change during charge/discharge processes [1-4]. Tremendous efforts have been made to overcome the energy storage limitation through synthesizing new materials and designing new capacitor configurations [5-9]. To achieve high energy density in supercapacitors, electrode materials are often required to exhibit large specific surface area and high electrical conductivity. Recently, pseudoactive materials are often integrated in electrodes to generate large redox current during charge/discharge processes. The major theme is to incorporate pseudoactive metal oxides [10-17] or conductive polymer nanostructures [18-24] into a conductive carbon matrix. With combined merits of pseudoactive materials (large faradic capacitance) and carbon (high conductivity and large specific surface area), these composite electrodes have demonstrated an enhanced electrochemical capacitance performance. To allow more electrolyte ions accessible to the active sites of the electrode surface and generate larger current density, porous or tubular-structured electroactive materials are attracting ever increasing attention in recent years. Most of the current methods to synthesize porous/tubular structures rely on the template method, and various porous nanostructures have been synthesized including Ni-NiO core-shell inverse opals [25], mesoporous Co_3O_4 [26], porous graphitic carbon [27], etc. However, this template approach usually suffers from high cost and complicated operations. Methods to prepare carbon based metal oxide nanocomposites include thermal decomposition [28,29], self-assembly [30,31], electrochemical deposition [32,33] and layer-by-layer technique [34]. Even though the nanostructures can be well controlled from these methods, they either are not highly efficient for scale-up production or require multiple skillful processes for successful synthesis. Until now, it is still a challenge to synthesize high-performance hybrid electrode materials from a facile and cost-effective process.

Microwave with its extremely fast heating and cooling rates has been demonstrated as a highly efficient energy source for the preparation of organics [35] and inorganic nanostructures [36-40]. The average microwave power absorption value or the heating potential [41] depends on the material dielectric property, microwave frequency, and the used electric field intensity [42-44]. For a given reaction, the reactants and intermediates can have different dielectric constants at different reaction stages. Microwaves can selectively interact with the intermediate in the transient state and overcome the

high activation energies for product formation [45,46]. Besides, the microwave heating reduces the overall thermal gradients and thus yields more uniform products in the reaction [47,48]. Our previous study has demonstrated the feasibility of using microwave energy to synthesize novel carbon/ $\text{Co}@/\text{Co}_3\text{O}_4$ hybrid structures for electrochemical energy storage [41]. This facile and cost effective method is very general and could be extended to prepare other hybrid materials for applications in various fields [49-51].

Besides the aforementioned electrode materials, many other factors including electrolyte, separator, and assembling structure of the capacitor affect its final performance in different ways. For example, organic electrolytes can provide a larger voltage window than regular aqueous electrolytes such as H_2SO_4 , KOH and Na_2SO_4 [2]. Researchers recently develop an asymmetrical electrode configuration using one carbon electrode and the other pseudoactive electrode, which gives higher energy and power density than their corresponding symmetric configuration [8,52]. All the efforts trying to improve the energy density and power density until now are all focusing on the inside of the capacitor including new electrode material synthesis and novel capacitor configuration design. Our previous research reveals that external magnetic field (MF) could enhance the capacitance of Fe_2O_3 /graphene nanocomposites significantly after applying a small external MF [10]. However, it is still not clear how external MF affects the electrochemical capacitance. It is critically important to reveal the underlying mechanism and guide future technology advancements in practical device applications.

Here, both conventional and microwave-assisted annealing methods are used to prepare magnetic microtubule nanocomposites (MMNs) from widely available starting materials of cotton fabric and inorganic salts including $\text{Fe}(\text{NO}_3)_3$, $\text{Ni}(\text{NO}_3)_2$, and $\text{Co}(\text{NO}_3)_2$. Products noted as Fe-M, Ni-M, Co-M and Fe-C, Ni-C, Co-C indicate that they are decorated with Fe, Ni and Co via microwave (M) and conventional (C) annealing, respectively. The nanostructure morphology and crystalline structure from both processes are comparatively investigated and their electrochemical energy storage properties are also evaluated. More importantly, a small external MF could affect the electrochemical properties of these 1D tubular hybrids significantly and the behind mechanisms are revealed from both experimental results and theoretical analysis.

Experimental

Magnetic microtubule nanocomposites preparation

The magnetic microtubule nanocomposites (MMNs) were prepared as follows. First, the commercially available cotton fabric (CF) was dried at 80°C in a regular oven for 6 h and immersed in 40 mL 1.0 M $\text{Fe}(\text{NO}_3)_3$, 1.0 M $\text{Ni}(\text{NO}_3)_2$ and 1.0 M

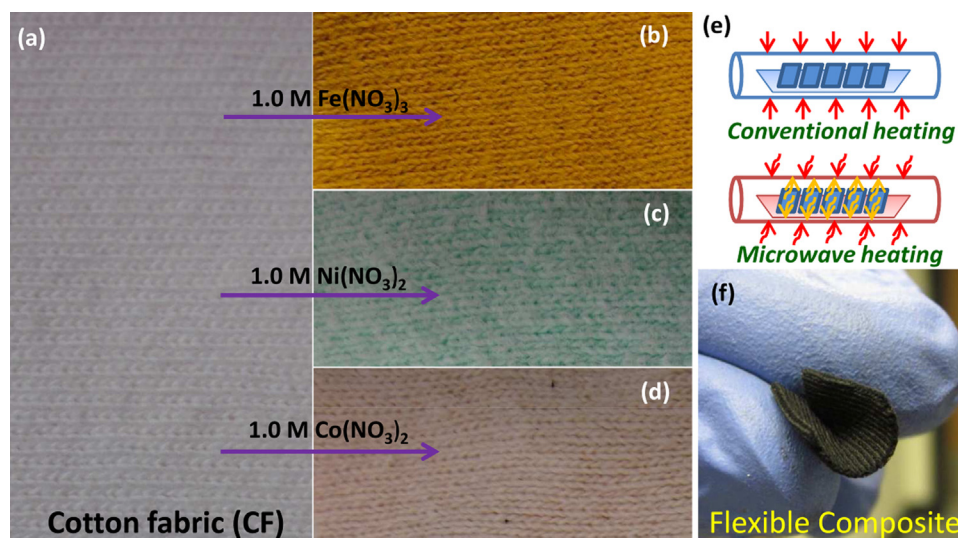


Figure 1 Photograph of (a) cotton fabric, and cotton fabric after immersing in salt solutions of (b) 1.0 M $\text{Fe}(\text{NO}_3)_3$, (c) 1.0 M $\text{Ni}(\text{NO}_3)_2$, and (d) 1.0 M $\text{Co}(\text{NO}_3)_2$, respectively. (e) Scheme of conventional heating and microwave heating used to manufacture magnetic microtubule nanocomposites in this work, and (f) the nanocomposite fabric still maintains its flexibility after thermal treatment.

$\text{Co}(\text{NO}_3)_2$ solution, respectively. After 2 h, the fabric was further impregnated at 700 mm Hg vacuum for 4 h. Then, the impregnated cotton fabrics were taken out of the solution and dried at 80 °C overnight. The photographs of the fabric before and after immersing in different inorganic salts are shown in Figure 1(a-d). Finally, the above prepared fabrics were thermally treated using microwave and conventional heating at 850 °C for 2 h in nitrogen atmosphere. The details of the annealing processes refer to our previous publication [53]. Both microwave and conventional heating schemes are shown in Figure 1(e). More importantly, the magnetic microtubule fabrics after thermal treatment still maintain its flexibility, Figure 1(f), which can be bent over without breakage. This is especially important for creating flexible energy storage devices.

Structure and property characterizations

The morphology of the MMNs was characterized using scanning electron microscopy (Hitachi S-3400 scanning electron microscopy). The TEM was done using JEOL 2010F with field-emission gun at 200 kV, which was equipped with a Gatan Image Filter for elemental mapping. The images and diffraction patterns were acquired using a Gatan Orius CCD camera. The powder X-ray diffraction analysis of the MMNs was carried out with a Bruker AXS D8 Discover diffractometer with GADDS (General Area Detector Diffraction System) operated with a $\text{Cu-K}\alpha$ radiation source filtered with a graphite monochromator ($\lambda=1.5406 \text{ \AA}$). The Raman spectra of MMNs were measured using a Horiba Jobin-Yvon LabRam HR Confocal Microscope with 633 nm (Laser Filter: D 0.3) laser excitation at 1.5 cm^{-1} resolution. The Raman spectrum was collected in the spectral region from 400 to 3000 cm^{-1} with a grating of 300 grooves/mm and confocal pinhole of 200 μm . The compositions of all the samples were analyzed by X-ray photoelectron spectroscopy (XPS). XPS measurements were conducted on a Kratos AXIS 165 system.

Analysis of each sample started with a quick survey scan in the binding energy range from 1200 to 0 eV at the pass energy level of 40 eV to check all the possible elements existing in the sample, followed by the high-resolution scan of each element at the pass energy level of 160 eV to obtain the compositional results. Both survey and high resolution scans were carried out with a Mono Al X-ray source at the anode of 10 kV and beam current of 15 mA. The magnetic properties of the MMNs at room temperature were measured in a 9 T physical properties measurement system (PPMS) by Quantum Design. Room temperature magnetoresistance (MR) was carried out on a compressed disk-shaped sample with the same composition of the electrode using a standard 4-probe technique.

Electrochemical characterization

The working electrodes were prepared by mixing 80 wt% sample (Fe-C, Fe-M, Ni-C, Ni-M, Co-C and Co-M) powders with 10 wt% acetylene black and 10 wt% polyvinylidene fluoride (PVDF) binder. The loading of the active materials on the nickel foam was calculated from the weight difference before and after loading the materials. The prepared electrode was soaked in 1.0 M KOH solution overnight before the electrochemical test. Electrochemical characterization was carried out in a three-electrode cell using platinum wire and Hg/HgO (SCE) as the counter and reference electrode, respectively. 1.0 M KOH was used as electrolyte. All electrochemical measurements were conducted using a VersaSTAT 4 potentiostat (Princeton Applied Research). Cyclic voltammograms (CV) measurements were performed at different voltage scan rates in a range from 5 to 100 mV/s. Galvanostatic charge/discharge measurements were carried out at different current density from 0.5 to 10.0 A/g. To test the electrochemical property of the MMNs in a magnetic field, the whole electrochemical cell was fixed between the two magnetic poles of an electromagnet

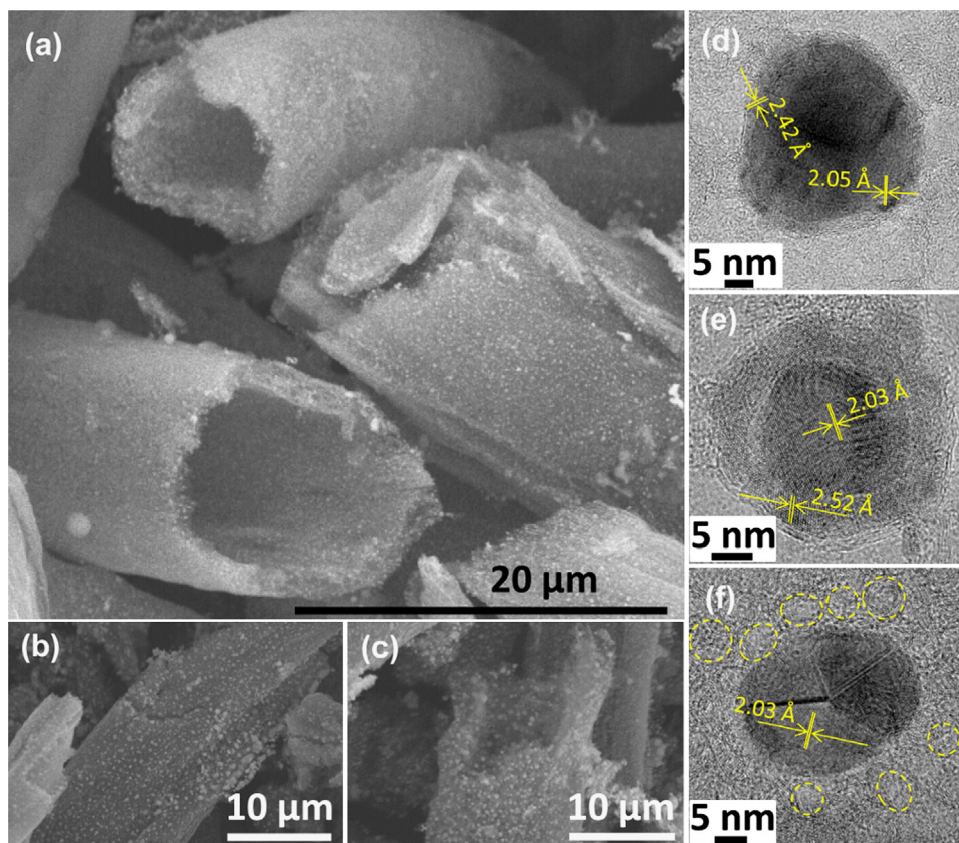


Figure 2 Microstructure of the MMNs. SEM of (a) Co-M, (b) Fe-M, and (c) Ni-M; high resolution TEM of typical individual (d) Co-M, (e) Fe-M, and (f) Ni-M nanoparticles.

(EM4-HVA H-Yoke, Lake Shore Cryotronics, Inc. USA). Testing fixture refer to our previous publication [10]. The magnetic field flux density can be controlled through tuning the magnitude of the current. In this work, the magnetic field strength was fixed at 0.072 T, which was measured by a Gauss/tesla meter (7010 Gauss/tesla Meter, Sypris).

Results and discussion

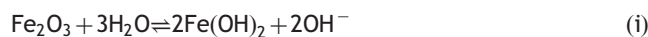
Figure 2(a-c) displays the SEM microstructures of Co-M, Fe-M and Ni-M, respectively. These images clearly show that the MMNs exhibit microtubular structure with an out-diameter of about 10.0-15.0 μm and wall thickness of 1.0-1.5 μm . The tube length can be easily extended to above hundred micrometers without breakage, Figure S1(a, c and e). More importantly, the MMNs fabrics still remain excellent flexibility, which is critically important for manufacturing wearable energy storage devices. It is observed that the nanoparticles have been successfully synthesized and are uniformly grown inside the carbon microtube wall as well as adhered to the wall surface. The average nanoparticle size for each composite is observed to be 30-50 nm. The nanostructure morphology and crystalline structure of the nanoparticles in each composite have been characterized using high resolution TEM, Figure 2(d-f). In Figure 2(d), the clear lattice fringes of 2.05 and 2.42 \AA indicate the Co (111) (PDF#15-0806) and Co_3O_4 (311) (PDF#42-1467) crystal planes. Nanoparticles with core-shell structure can be

clearly observed in Fe-M, Figure 2(e), where the shell inter-layer distance of 2.52 \AA corresponds to Fe_2O_3 (311), and the core interlayer distance of 2.03 \AA corresponds to Fe (110) (PDF#39-1346). Highly crystalline Ni (111) (PDF#00-004-0850) and porous graphitized carbon (marked with dash circle) are observed in Ni-M, Figure 2(f). All these results confirm the efficient conversion of inorganic salt to crystalline magnetic nanoparticles using microwave energy. Under conventional annealing, similar microtubule structures could be obtained except that the Ni-C shows a much rougher surface, Figure S1(d). These MMNs are able to offer much larger specific surface area than the corresponding solid structures, which allow more metal oxide nanoparticles participating in the electrochemical reaction and potentially generate larger capacitance. Besides, the tubular structure provides additional micro-channels for electrolyte ions diffusion and thus facilitates the electron transfer at the electrode/electrolyte interface. Benefits from the hybrid structure, the carbon matrix serves as a cushion to reduce the structural damage from the volume change of the nanoparticles during the charge/discharge process, and thus yields a potential long-term cycling stability. Raman spectra show the typical D, G and 2D bands of graphitized carbon, Figure S2, indicating the cotton fabric has been completely converted to graphitized carbon from both microwave and conventional annealing processes. The crystalline structure and oxidation states of the nanoparticles have been further verified by X-ray diffraction (XRD, Figure S3) and X-ray photoelectron spectroscopy (XPS, Figure S4) techniques.

XRD results indicate that the Co-M and Co-C exhibit similar cobalt (111) and (200) crystalline planes (PDF#15-0806). The existence of Co_3O_4 has been verified by Raman spectra, Figure S2(B). With regard to Fe and Ni doped composites, Fe (110 and 100) and Ni (111 and 200) crystalline peaks are observed in Fe-M and Ni-M, respectively. Even though the oxides cannot be clearly detected by XRD, the XPS evidence (Figure S4) proves the existence of Fe_2O_3 and NiO in Fe-M and Ni-M, respectively. Using conventional annealing, additional Fe_2O_3 and NiO crystalline peaks from XRD diffraction patterns are observed in Fe-C and Ni-C, respectively, Figure S3(b and d).

To evaluate the performance of these hybrid electrode architectures in supercapacitor applications, the electrochemical tests were carried out with a three-electrode configuration. The electrode preparation and testing details are provided in the Supporting information, S1.4. The same cell configuration was then placed in a small external MF of 0.072 T to study the MF effect on the electrochemical performance. Figure 3(a) shows the cyclic voltammograms (CVs) of the Fe-M, Ni-M and Co-M at a voltage scan rate of 20 mV/s. The shape of the CV curves for these MMNs indicates that the capacitive characteristic is a typical pseudocapacitor, which is different from that of an electric double-layer capacitor (EDLC) that exhibits a rectangular CV curve [2]. Pairs of well-defined cathodic and anodic peaks

are clearly observed over the entire potential range from -0.3 to 0.5 V, Figure 3(a). Typically, Fe-M and Ni-M show symmetric CV curve and single redox peak, indicating a reversible reaction occurred on each electrode:



[54,55]

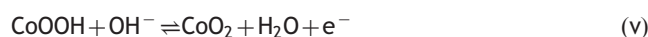


[56]

Co-M gives two redox peaks, which correspond to the reversible reactions between different cobalt oxide states according to the following reactions:



[57,58]



CV is one of the most important techniques for investigating the effect of MF on redox reactions and mass transport processes such as convection, diffusion, and migration [59,60]. When MF is externally imposed on an electrochemical unit, the mass transport of electrolyte at the electrolyte/electrode interface is altered, which

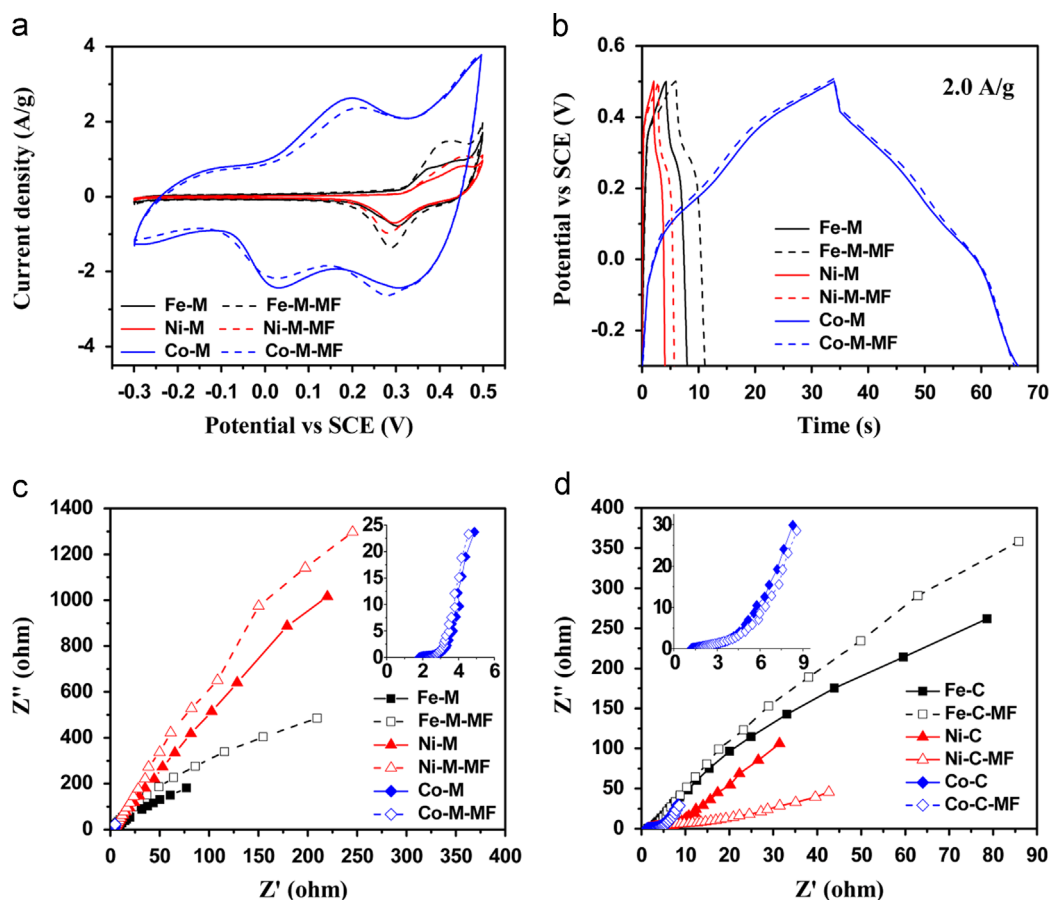


Figure 3 Electrochemical performance of Fe-M, Ni-M and Co-M electrodes with/without MF. (a) Cyclic voltammograms at a voltage scanning rate of 20 mV/s, (b) galvanostatic charge/discharge curves at a current density of 2.0 A/g, (c) Nyquist plot of Fe-M, Ni-M and Co-M, and (d) Nyquist plot of Fe-C, Ni-C and Co-C. Solid lines were measured in normal condition and dash lines were measured with the presence of MF.

changes the electrical double layer at the electrode surface [60]. These changes are mainly attributed to the magneto-hydrodynamic (MF generates current in a moving conductive fluid, which in turn creates forces on the fluid and the MF) phenomenon, which accelerates the ion transportation rate within the electrolyte solution and the electron exchange at the electrolyte/electrode interface [61]. The CV curves in MF, as indicated by dash lines in Figure 3(a), show an obviously enlarged current density of the redox peaks in Fe-M and Ni-M. These results reveal that more electrolyte ions transport to the electrode surface with the assistance of the applied MF. The additional electrolyte ions are induced by the disturbed electrolyte transport process due to the significant interaction between MF and the electric double layer structure [59]. A similar increased charge transfer current within MF was also observed in a copper deposition process [62,63]. Less obvious effect of MF is observed on Co-M that the dash line deviates from the solid line slightly. In addition, the anodic peaks in MF are shifted to positive potential (Fe-M: 0.377-0.421 V; Ni-M: 0.454-0.457 V; Co-M: 0.198-0.214 V, second anodic peak is out of scanning potential range) while the cathodic peaks are shifted toward negative potential (Fe-M: 0.302-0.289 V; Ni-M: 0.299-0.285 V; Co-M: 0.307/0.03-0.283/0.026 V). Different from the microwave annealed samples, the conventionally annealed Ni-C exhibits much larger CV current density than Fe-C, Figure S5(a). In addition, the MF even splits a single reduction peak into two different peaks, indicating that another oxidation product, Ni_2O_3 , is also formed together with NiOOH during the oxidation reaction. The Co-C only shows one pair of redox peak and the CV curve shape is significantly different from that of Co-M. These unique phenomena reveal that both the annealing method in material preparation and the applied MF during electrochemical characterization could significantly change the electrochemical behavior of these MMNs.

Figure 3(b) shows the galvanostatic charge-discharge curves of MMNs measured at a current density of 2.0 A/g within the potential range of -0.3 to 0.5 V. The discharge curves display a small potential drop at the very beginning of the discharge process, which was caused by the internal resistance of the electrode [64]. The subsequent slower potential decay demonstrates the pseudocapacitive feature of the electrode that is responsible for longer discharge duration. Apparently, the charge/discharge duration of Fe-M and Ni-M is longer after applying the MF, which is consistent with the enlarged CV area in Figure 3(a). The MF increases the discharge time of Fe-C as expected that is similar to Fe-M, while it surprisingly decreases the discharge time of Co-C obviously, Figure S5(b). The charge/discharge curve of Co-M in MF is almost overlapped with the one in regular condition, indicating that the MF has negligible influence on Co-M at the current density of 2.0 A/g. However, it does not necessarily mean that the MF has negligible influence on Co-M at other testing conditions. A systematic study has been conducted and discussed in the following sections.

Electrochemical impedance spectroscopy (EIS) was examined in Figure 3(c and d) to better understand the electrochemical behavior of the MMNs. The Fe-M and Ni-M show much larger impedance (Figure 3c) than Co-M (inset of Figure 3c), revealing the larger internal resistance of Fe-M

and Ni-M. This well explains their lower current density in the CV curves than Co-M as well as their shorter discharge durations since the low resistance is required for obtaining higher discharge duration. With the presence of MF, the EIS curve for each composite even shifts towards higher resistance value, which is attributed to the magnetoresistance (MR, defined as resistance change under an applied MF [65-67]) phenomena. To study the resistance change of each electrode after exposing to MF, the MR measurement was conducted on electrodes, which were pre-dipped by electrolyte (1.0 M KOH) to mimic the real electrochemical testing condition, Figure 4. Since very small MF of 0.072 T has been applied, the MR behavior at low field is more indicative in current study. Most of the electrodes including Fe-M, Fe-C, Ni-M and Co-M are observed to exhibit large positive MR (resistance increases with increasing MF), the resistance increased by upto $\sim 6\%$ in large MF of 9.0 T. The Co-C shows a negative MR, indicating that the resistivity decreases with increasing MF. More interestingly, the MR of Ni-C continuously decreases to -0.8% with increasing field to 4.0 T. After that, MR increases gradually to positive and reaches 2% at MF of 9.0 T. As aforementioned, low resistance electrodes are normally required to achieve high capacitance. It seems that the external MF is going to decrease the capacitance since the resistance has been increased after applying MF except for Co-C and Ni-C (at low MF). However, the enlarged CV area and elongated discharge time (Fe-M, Fe-C and Ni-M) reveal the enhanced capacitance with the presence of MF. Therefore, MF may affect the electrochemical unit in some other ways, and contributes to the capacitance enhancement rather than MR behavior of the electrodes.

To further explore the MF effect on the capacitance, an equivalent circuit is explored to fit the impedance spectra with the aim to disclose the internal resistance change of the electrochemical system upon applying MF, Figure S6. The fitting results for the three internal resistances,

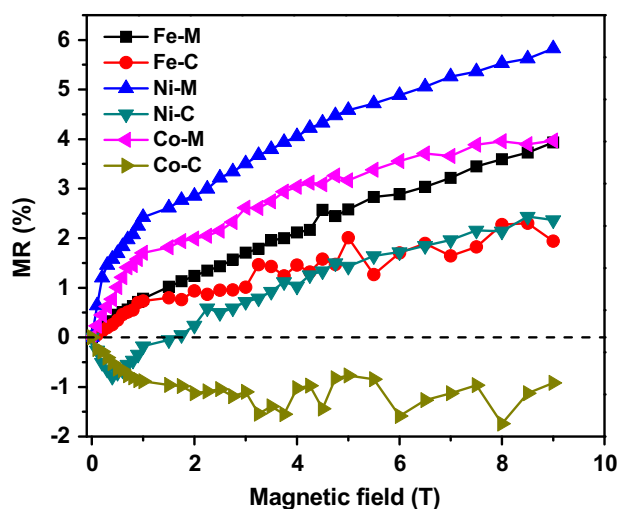


Figure 4 MR behavior of Fe-M, Fe-C, Ni-M, Ni-C, Co-M, and Co-C at 290 K. Disk shaped samples were prepared by mixing 80 wt% electroactive materials (Fe-C, Fe-M, Ni-C, Ni-M, Co-C and Co-M) powders with 10 wt% acetylene black and 10 wt% polyvinylidene fluoride (PVDF) binder. The samples were immersed in 1.0 M KOH electrolyte overnight before testing to mimic the real electrochemical condition.

solution resistance in bulk electrolyte R_s , electrode/electrolyte interfacial charge transfer resistance R_{ct} , and low frequency leakage resistance R_{leak} (resistance of small leakage current flowing across the double layer at the electrode-electrolyte interface) are summarized in Table 1. The scheme of the capacitance internal resistances is illustrated in Figure 5(a). Without MF, the electrolyte ions transport towards the electrode surface under an electrostatic force. While in MF, additional Lorentz force will be applied on the moving ions transverse to the magnetic field lines, which is also called magnetohydrodynamic phenomenon. Consequently, the electrolyte ions will move following a circular pattern towards the electrode surface, which actually brings electrolyte convection in the bulk electrolyte and thus reduces the R_s . The simulation results in Table 1 further confirm this phenomenon that decreased R_s

Table 1 Simulated results of electric impedance spectra in normal condition and in MF.

Sample	Simulated internal resistance (ohm)					
	R_s	R_s -MF	R_{ct}	R_{ct} -MF	R_{leak}	R_{leak} -MF
Fe-M	1.25	1.10	8.95	27.98	140.50	282.80
Fe-C	1.38	1.26	19.46	22.10	103.00	212.20
Ni-M	1.99	1.80	9.48	26.95	84.76	388.30
Ni-C	1.69	1.44	10.03	1.27	479.30	43.33
Co-M	1.80	1.60	1.06	1.88	1.22	0.63
Co-C	1.33	1.23	5.81	2.07	249.10	288.00

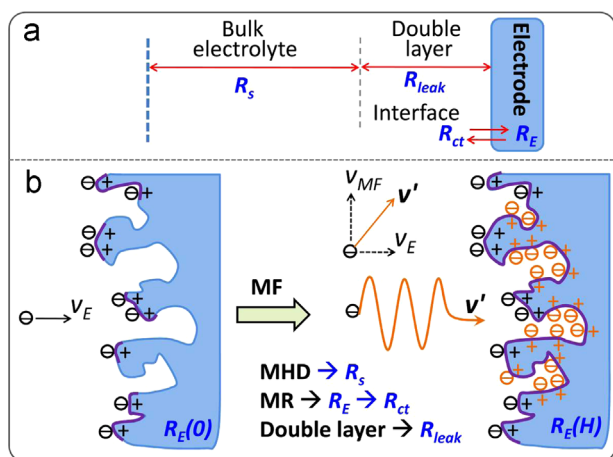


Figure 5 Schematic illustration of (a) capacitor internal resistances include solution resistance R_s in bulk electrolyte, leakage resistance R_{leak} in double layer region and charge transfer resistance R_{ct} at electrode/electrolyte interface, R_E is the electrode resistance and (b) internal electron transportation before and after applying a magnetic field. V_E represents the electrolyte ion transportation under electrostatic force, V_{MF} represents ion transportation with Lorentz force in MF, V' is the ion transportation under electrostatic force and Lorentz force. The purple curvature at electrode surface represents the double layer area. Magnetohydrodynamic, magnetoresistance (MR), electrode resistance without MF, $R_E(0)$, electrode resistance with a field H , $R_E(H)$.

has been observed in all electrodes after applying MF. This MF induced electrolyte convection also pushes the electrolyte ions deeper to reach extra electrode surface areas that are not accessible in a conventional approach, Figure 5(b). The enlarged active surface area causes two major benefits of (1) helping to generate larger specific capacitance of the electrodes; (2) building up a complete double layer that restricts free electrons passing through the double layer and thus increasing the R_{leak} . This is the reason for the observed capacitance enhancement in Fe-C, Fe-M, Ni-C and Ni-M electrodes. R_{ct} reflects the resistance at electrode surface, which is closely related to the resistance of the electrode itself (R_E). Positive MR means that R_E increases with increasing MF, $R_E(H) > R_E(0)$, and negative MR indicates $R_E(H) < R_E(0)$. Experimental results in Figure 4 reveal that Fe-M, Fe-C, Ni-M and Co-M show positive MR at low field, which is highly consistent with the simulation results of the increased R_{ct} after applying MF, Table 1. In addition, the two electrodes of Ni-C and Co-C, showing negative MR at low MF, give reduced R_{ct} as predicted by theory. These results confirm that the MR characteristics of the electrodes play a significant role in interfacial charge transfer during charge/discharge. The leakage resistance, R_{leak} , is much more complex in these carbon/metal oxide pseudoactive electrodes than that of pure carbon electrode. Two contrary contributions are involved. One is positive contribution from electrolyte convection that helps to build up the double layer and thus increases R_{leak} . On the other side, pseudoactive metal oxide involves Faradaic current passing through the double layer during charge/discharge and therefore decreases the R_{leak} . Either enhanced R_{leak} or reduced R_{leak} is observed, Table 1, depending on a variety of factors such as the specific surface area of electrodes, ratio of metal oxide to carbon, pseudoactivity of the metal oxides etc.

The final capacitive performance of the electrodes is determined by the total internal resistance and fraction of contribution from each of the three resistance terms. Generally, after applying a small external MF, the smaller R_s , R_{ct} and larger R_{leak} are helpful to improve the energy storage performance. In this work, the slightly reduced R_s in MF does not account for the significant change of capacitance. The R_{ct} and R_{leak} dominate the interfacial charge carrier exchange between electrode and electrolyte at the electrode surface. This is especially true for pseudoactive electrodes that redox reactions dominate the electron transfer at electrode surface.

Figure 6(a) shows the specific capacitance of each MMNs calculated at different voltage scan rates using Eq. (1)

$$C_s = \frac{\int idV}{2 \times m \times \Delta V \times S} \quad (1)$$

where C_s is the specific capacitance in F/g, $\int idV$ is the integrated area of the CV curve, m is the mass of the electrode material in g, ΔV is the scanned potential window in V, and S is the scan rate in V/s. The CV curves of each electrode at different voltage scan rates are displayed in Figures S7-S9. Co-M exhibits relatively higher capacitance than other materials at various voltage scan rates except that Co-C reaches the highest capacitance of 100.0 F/g at a scan rate of 5 mV/s. Microwave annealing helps to attain higher capacitance of Fe and Co doped electrodes, while conventional annealing is more favorable for producing high capacitive Ni doped electrodes. Different from Fe and Ni

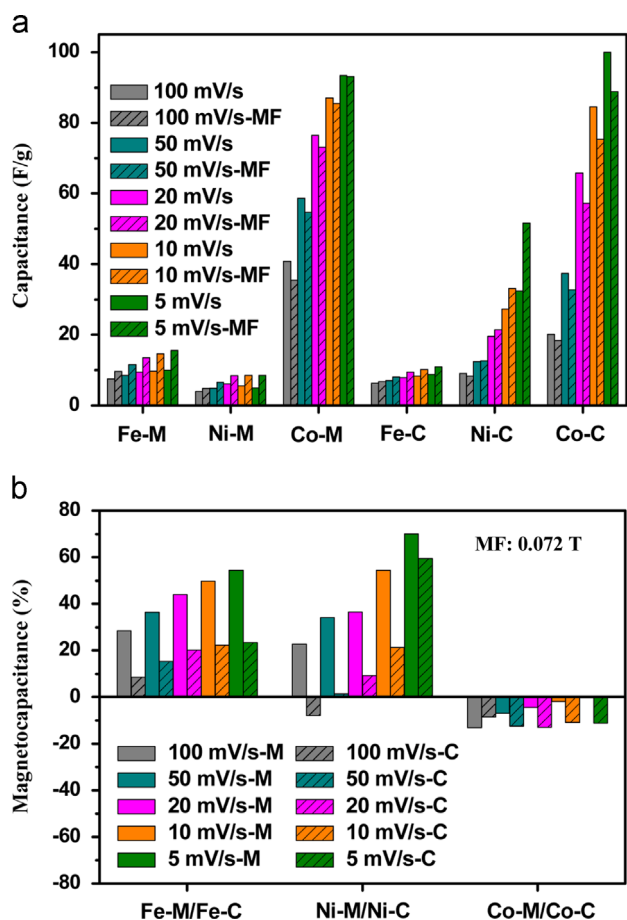


Figure 6 (a) Specific capacitance of MMNs at different voltage scanning rates, (b) MF induced capacitance change of MMNs at different scanning rates.

doped MMNs where MF has significantly enhanced the capacitance at different scan rates (except Ni-C at a scan rate of 100 mV/s), Co-M and Co-C show an opposite trend that their capacitance decreases after applying MF, **Figure 6(a)**. **Figure 6(b)** illustrates the MF effect on the capacitance variation for each material at different scan rates. Magnetocapacitance (MC) is defined as the ratio of capacitance change after applying a magnetic field to the capacitance without MF. MC was used as an indicator to quantify the MF effect on electrode capacitance that can be calculated using Eq. (2):

$$MC = \frac{C_s(H) - C_s(0)}{C_s(0)} \times 100\% \quad (2)$$

where $C_s(H)$ is the capacitance obtained with an applied external MF of H in F/g, $C_s(0)$ is the capacitance without MF in F/g. The Fe and Ni doped electrodes annealed from both microwave and conventional processes exhibit similar patterns that the MC increases with decreasing the scan rate. Moreover, the microwave annealed materials (Fe-M and Ni-M) are more sensitive to MF and the MC is much higher than the conventional annealed materials (Fe-C and Ni-C). Noticing that the MF even decreases the capacitance of Ni-C at a high scanning rate of 100 mV/s, i.e., $MC < 0$. Similar phenomena are more obviously observed in Co-M and Co-C that MF decreases the capacitance by less than 15% at all scan rates. All these results indicate that the MF effect on the

electrochemical process is related to both the electrode materials and the electrochemical testing conditions. Even though these MMNs acquire different saturated magnetization, coercivity and electrical conductivity, **Figures S10 and S11**, a solid correlation between magnetic property and MC performance could not be obtained.

Energy density (E) and power density (P) of the electrode materials are calculated from Eqs. (3) and (4) [68].

$$E = \frac{1}{2} C_s (\Delta V)^2 \quad (3)$$

$$P = \frac{E}{t} \quad (4)$$

where C_s is the specific capacitance calculated from the charge/discharge curve in F/g, ΔV is the potential drop during discharge in V, E is the energy of the electrode in Wh/kg, and t is the discharge time in h. All the electrode materials can be divided into two groups, one is distributed in the double layer capacitor region in **Figure 7**, typically Fe-C, Fe-M and Ni-M, the energy density level is similar to double layer capacitor and can be increased after applying MF. The other group, Ni-C, Co-M and Co-C, obtains an energy density larger than double layer capacitors and ultracapacitors. While Ni-C exhibits a tremendous energy drop at high power density, indicating its unstable rate performance [69,70]. The high power density is attributed to the fast kinetic reaction between electrolyte ions and electrode, which arose from the hollow tubular structure of the nanocomposites that permits a fast diffusion of electrolyte ions to reach the active sites and provides a short diffusion distance to accelerate the reaction. The experimental results were compared with data from other energy storage units such as lead-acid battery, double layer capacitors, ultra capacitors and conventional capacitors, **Figure 7** [68,71]. The Ni-C, Co-C and Co-M electrodes demonstrate much higher energy density than double layer capacitors, ultra capacitors and comparable to lead-acid batteries, but significantly larger power density than batteries. Besides, the

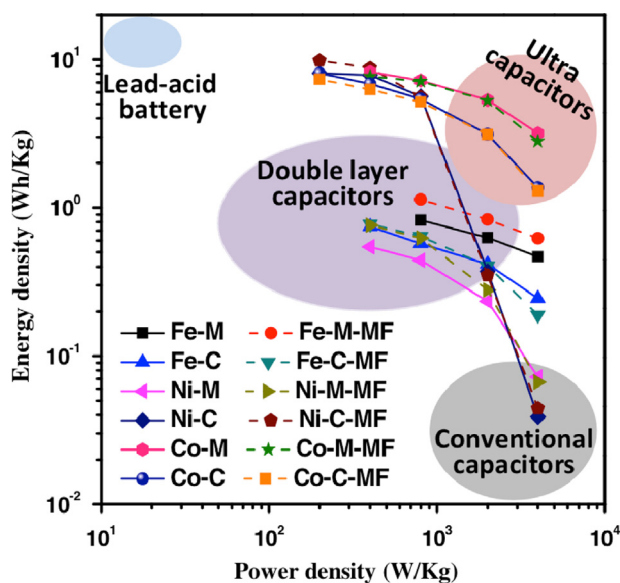


Figure 7 The Ragone plot of the nanocomposite electrode. Circled symbols indicate the energy density-power density maps for existing energy storage systems for comparison.

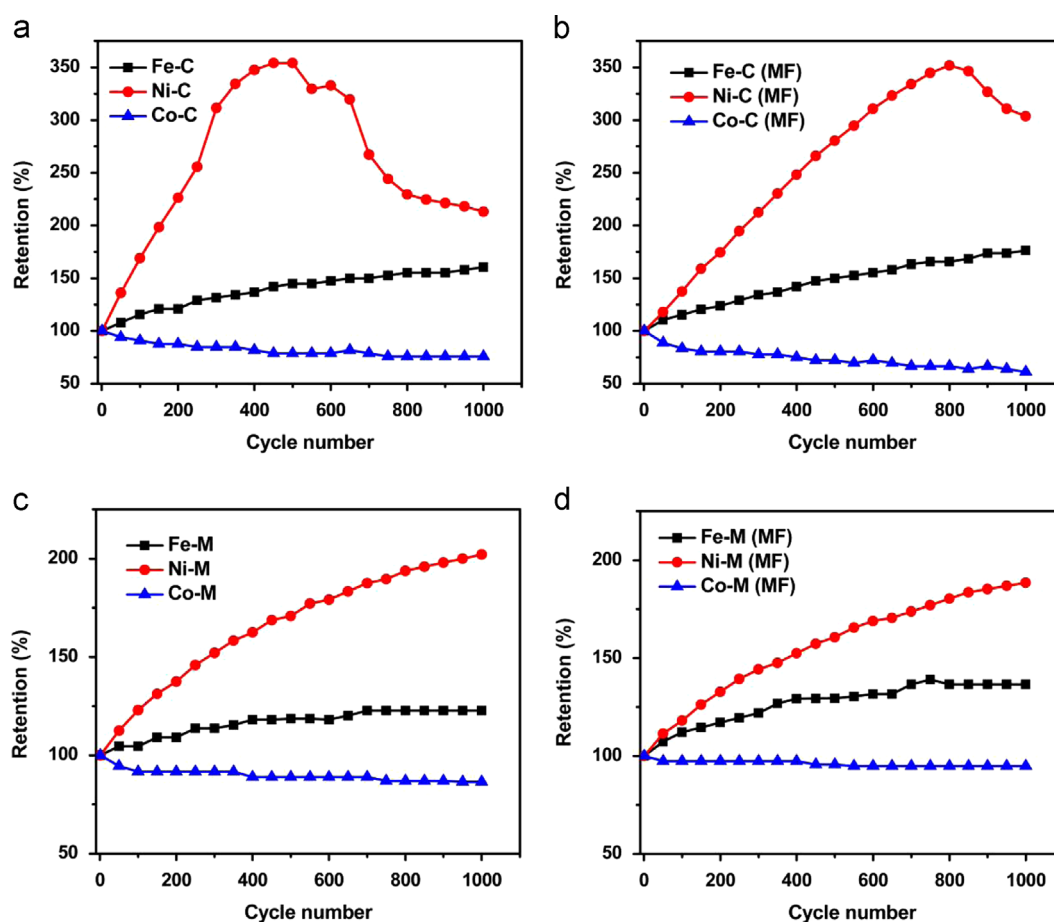


Figure 8 Cycling stability of (a) Fe-C, Ni-C and Co-C, (b) Fe-C, Ni-C and Co-C in MF, (c) Fe-M, Ni-M and Co-M, (d) Fe-M, Ni-M and Co-M in MF.

economic raw materials, facile processing technique and satisfactory capacitance performance make these nanocomposite electrodes advantageous over others in terms of manufacturing cost and long term stability. These results suggest a promising electrode material that may lead to a new class of energy storage devices.

The long-term cycling stability of the electrode materials is another critical requirement for practical applications. Figure 8(a and c) depicts the capacitance retention as a function of the cycle number at a current density of 2.0 A/g for upto 1000 cycles. The cycling performance of the electrodes with MF is also studied to determine how the MF affects the energy storage property in the long term, Figure 8(b and d). All the electrodes show three major retention phenomena: (1) retention increases with increasing the cycle number, for example, Fe-C, Fe-M and Ni-M; (2) retention increases initially to a maximum value and then decreases gradually with increasing the cycle number, Ni-C; (3) retention decreases with increasing the cycle number, such as Co-C and Co-M. The observed retention increase in Fe-C, Fe-M and Ni-M is attributed to the gradual activation (oxidation) of the electroactive materials. The oxidized FeOOH and NiOOH are amorphous, where OH⁻ ions could easily penetrate into the inner area of the magnetic particles [72]. Therefore, more metal components will be oxidized to active metal oxides, which allow more oxides participate in the reaction and lead to larger capacitance. Similar activation phenomenon has also

been observed in NiCo₂O₄ [73]. The metal oxidation of Fe-M after cycling test has been evidenced by the selected area electron diffraction (SAED) patterns as revealed in Figure 9(a and b). The SAED pattern clearly indicates the Fe(110) and Fe(220) crystal planes before cycling, Figure 9(a). After cycling, the SAED pattern shows extra Fe₂O₃ crystal planes (211), (430) and (444) together with Fe(110) plane, Figure 9(b), revealing an obvious oxidation after 1000 charge/discharge cycles. This result has also been confirmed by energy filtered TEM results, Figure S12(a-c), where oxidation occurs from upright site of the particle and then diffuses to lower left. Meanwhile, it is observed that the retention curve increases continuously and seems unsaturated even after 1000 cycles, which is due to the good protection of carbon shell that prevents the direct contact of metal part and electrolyte ions, Figure 9(c) and Figure S12(d-f). Ni-C shows interesting retention saturation at cycle number of around 500 and then retention decrease afterwards, Figure 8(a). This result indicates that the pure Ni metal part of the nanoparticles has been completely oxidized after 500 cycles and then degradation occurs due to the structural damage during charge/discharge, Figure S13(b). Even though, the retention is still maintained above 200% after 1000 cycles. Co-M and Co-C show only retention decrease, Figure 8(a and c). As mentioned above, two reversible reactions are involved during redox reaction, where CoOOH served as an intermediate between Co₃O₄ and CoO₂. Even though the CoOOH is still penetrable to the

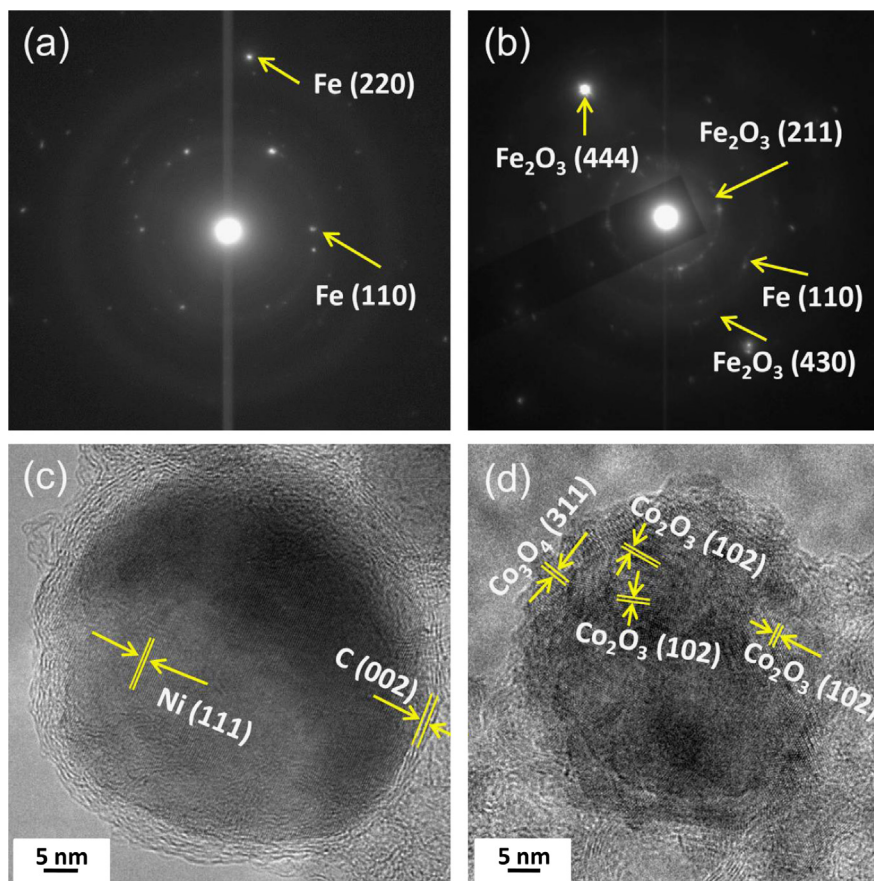


Figure 9 Selected area electron diffraction pattern of Fe-M (a) before cycling and (b) after 1000 cycling test. HRTEM of (c) Ni-M and (d) Co-M after 1000 cycling tests.

OH^- ions and allows the oxidation occur, the oxidation product is mainly non-electroactive Co_2O_3 , **Figure 9**(d). In other words, the oxidation product does not contribute to the performance enhancement. On the contrary, the formed Co_2O_3 sacrifices the conductivity of the electrode. Therefore, only retention decrease has been observed.

With the existence of MF, the retention performance of each electrode has been changed but following the same pattern as the one without MF. Fe-C and Fe-M show larger retention of 176% and 137% with MF at 1000th cycle than that of 160% and 123% without MF, respectively. While for Ni-C and Ni-M, the MF slows down the oxidation process. Maximum saturation retention of 350% (same as the value without MF) is observed in Ni-C with MF, but the saturation peak delays to the 800th cycle. After that, similar retention degradation appears but with a higher retention value of 300% than 200% for the Ni-C under normal condition at 1000th cycle. Slower oxidation is also observed in Ni-M that the retention at 1000th cycle reaches 189% with MF, which is relatively smaller than that of 202% without MF. Co-M (>87%) acquires much larger retention as compared to Co-C (<76%) with MF or without MF. Especially, MF helps to further increase the retention of Co-M from 87% to 95%.

Conclusions

In conclusion, a new and cost-effective strategy has been successfully developed to produce flexible magnetic

microtubule nanocomposite fabrics for supercapacitor electrode applications. The hybrid structural design concept is very general and can be readily applied to other materials, such as manganese oxide, ruthenium oxide, to build nano- and micron- hybrid structures with high capacitance performance, which will be promising for a large spectrum of energy device applications. MF could either increase or decrease the capacitance of electrodes, depending on the interplay between MF and capacitor internal resistances. Electrodes prepared from microwave assisted annealing show higher magnetocapacitance and capacitance retention than the ones prepared from conventional annealing. Magnetic field induced magnetohydrodynamic phenomena in bulk electrolyte and magnetoresistance behavior of electrode are the main reasons for the tuned solution resistance and charge transfer resistance. In this work, a small external MF induced capacitance enhancement of upto $\sim 70\%$ has been revealed in nickel oxide doped carbon nanocomposite fabrics. This phenomenon promises a significant impact of this discovery in the energy storage field.

Acknowledgment

This project is supported by the Research Enhancement Seeded Grant from Lamar University. Partial financial supports from National Science Foundation, USA - Nanomanufacturing (CMMI 13-14486) managed by Dr. Bruce M. Kramer, Nanoscale Interdisciplinary Research Team and Materials

Processing and Manufacturing (CMMI 10-30755) managed by Dr. Mary M. Toney and Chemical and Biological Separations (CBET-1137441) managed by Dr. Rosemarie D. Wesson are kindly acknowledged. The authors appreciate the kind help from Dr. Amanda H. Young at Texas A&M University for the Raman characterization of the materials.

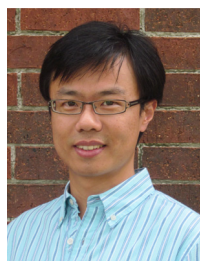
Appendix A. Supporting information

Supplementary data associated with this article can be found in the online version at <http://dx.doi.org/10.1016/j.nanoen.2014.04.002>.

References

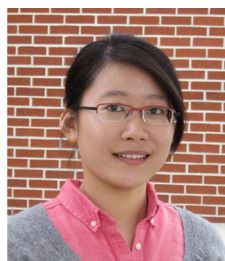
- [1] L.L. Zhang, X.S. Zhao, *Chem. Soc. Rev.* 38 (2009) 2520-2531.
- [2] G. Wang, L. Zhang, J. Zhang, *Chem. Soc. Rev.* 41 (2012) 797-828.
- [3] Y. Li, B. Tan, Y. Wu, *Nano Lett.* 8 (2007) 265-270.
- [4] A.S. Arico, P. Bruce, B. Scrosati, J.-M. Tarascon, W. van Schalkwijk, *Nat. Mater.* 4 (2005) 366-377.
- [5] Y. Zhu, S. Murali, M.D. Stoller, K.J. Ganesh, W. Cai, P.J. Ferreira, A. Pirkle, R.M. Wallace, K.A. Cychoz, M. Thommes, D. Su, E.A. Stach, R.S. Ruoff, *Science* 332 (2011) 1537-1541.
- [6] M.D. Stoller, C.W. Magnuson, Y. Zhu, S. Murali, J.W. Suk, R. Piner, R.S. Ruoff, *Energy Environ. Sci.* 4 (2011) 4685-4689.
- [7] M.D. Stoller, S. Park, Y. Zhu, J. An, R.S. Ruoff, *Nano Lett.* 8 (2008) 3498-3502.
- [8] L. Bao, X. Li, *Adv. Mater.* 24 (2012) 3246-3252.
- [9] Q. Lu, M.W. Lattanzi, Y. Chen, X. Kou, W. Li, X. Fan, K.M. Unruh, J.G. Chen, J.Q. Xiao, *Angew. Chem. Int. Ed.* 50 (2011) 6847-6850.
- [10] J. Zhu, M. Chen, H. Qu, Z. Luo, S. Wu, H.A. Colorado, S. Wei, Z. Guo, *Energy Environ. Sci.* 6 (2013) 194-204.
- [11] G. Yu, L. Hu, M. Vosgueritchian, H. Wang, X. Xie, J.R. McDonough, X. Cui, Y. Cui, Z. Bao, *Nano Lett.* 11 (2011) 2905-2911.
- [12] J. Mu, B. Chen, Z. Guo, M. Zhang, Z. Zhang, P. Zhang, C. Shao, Y. Liu, *Nanoscale* 3 (2011) 5034-5040.
- [13] A.L.M. Reddy, M.M. Shaijumon, S.R. Gowda, P.M. Ajayan, *Nano Lett.* 9 (2009) 1002-1006.
- [14] Y. Wang, H.J. Zhang, L. Lu, L.P. Stubbs, C.C. Wong, J. Lin, *ACS Nano* 4 (2010) 4753-4761.
- [15] J. Bae, M.K. Song, Y.J. Park, J.M. Kim, M. Liu, Z.L. Wang, *Angew. Chem. Int. Ed.* 50 (2011) 1683-1687.
- [16] F. Xia, X. Hu, Y. Sun, W. Luo, Y. Huang, *Nanoscale* 4 (2012) 4707-4711.
- [17] J. Zhu, M. Chen, Q. He, L. Shao, S. Wei, Z. Guo, *RSC Adv.* 3 (2013) 22790-22824.
- [18] Y.G. Wang, H.Q. Li, Y.Y. Xia, *Adv. Mater.* 18 (2006) 2619-2623.
- [19] Q. Wu, Y. Xu, Z. Yao, A. Liu, G. Shi, *ACS Nano* 4 (2010) 1963-1970.
- [20] L.Z. Fan, Y.S. Hu, J. Maier, P. Adelhelm, B. Smarsly, M. Antonietti, *Adv. Funct. Mater.* 17 (2007) 3083-3087.
- [21] D.-W. Wang, F. Li, J. Zhao, W. Ren, Z.-G. Chen, J. Tan, Z.-S. Wu, I. Gentle, G.Q. Lu, H.-M. Cheng, *ACS Nano* 3 (2009) 1745-1752.
- [22] M. Hughes, G.Z. Chen, M.S.P. Shaffer, D.J. Fray, A.H. Windle, *Chem. Mater.* 14 (2002) 1610-1613.
- [23] J. Zhu, M. Chen, H. Qu, X. Zhang, H. Wei, Z. Luo, H.A. Colorado, S. Wei, Z. Guo, *Polymer* 53 (2012) 5953-5964.
- [24] H. Wei, J. Zhu, S. Wu, S. Wei, Z. Guo, *Polymer* 54 (2013) 1820-1831.
- [25] J.-H. Kim, S.H. Kang, K. Zhu, J.Y. Kim, N.R. Neale, A.J. Frank, *Chem. Commun.* 47 (2011) 5214-5216.
- [26] X.-H. Xia, J.-P. Tu, X.-L. Wang, C.-D. Gu, X.-B. Zhao, *Chem. Commun.* 47 (2011) 5786-5788.
- [27] D.-W. Wang, F. Li, M. Liu, G.Q. Lu, H.-M. Cheng, *Angew. Chem.* 120 (2008) 379-382.
- [28] J. Zhu, S. Wei, H. Gu, S.B. Rapole, Q. Wang, Z. Luo, N. Haldolaarachchige, D.P. Young, Z. Guo, *Environ. Sci. Technol.* 46 (2012) 977-985.
- [29] J. Zhu, H. Gu, S.B. Rapole, Z. Luo, S. Pallavkar, N. Haldolaarachchige, T.J. Benson, T.C. Ho, J. Hopper, D. P. Young, S. Wei, Z. Guo, *RSC Adv.* 2 (2012) 4844-4856.
- [30] J. Li, S. Tang, L. Lu, H.C. Zeng, *J. Am. Chem. Soc.* 129 (2007) 9401-9409.
- [31] D. Wang, R. Kou, D. Choi, Z. Yang, Z. Nie, J. Li, L.V. Saraf, D. Hu, J. Zhang, G.L. Graff, J. Liu, M.A. Pope, I.A. Aksay, *ACS Nano* 4 (2010) 1587-1595.
- [32] E.S. Steigerwalt, G.A. Deluga, C.M. Lukehart, *J. Phys. Chem. B* 106 (2002) 760-766.
- [33] J. Yan, H. Zhou, P. Yu, L. Su, L. Mao, *Electrochem. Commun.* 10 (2008) 761-765.
- [34] N. Du, H. Zhang, B.D. Chen, X.Y. Ma, Z.H. Liu, J.B. Wu, D.R. Yang, *Adv. Mater.* 19 (2007) 1641-1645.
- [35] A. de la Hoz, A. Diaz-Ortiz, A. Moreno, *Chem. Soc. Rev.* 34 (2005) 164-178.
- [36] R. Harpeness, A. Gedanken, *Langmuir* 20 (2004) 3431-3434.
- [37] A.B. Panda, G. Glaspell, M.S. El-Shall, *J. Am. Chem. Soc.* 128 (2006) 2790-2791.
- [38] F. Bensebaa, F. Zavaliche, P. L'Ecuyer, R.W. Cochrane, T. Veres, *J. Colloid Interface Sci.* 277 (2004) 104-110.
- [39] W.-W. Wang, Y.-J. Zhu, *Mater. Res. Bull.* 40 (2005) 1929-1935.
- [40] Y.-J. Zhu, W.-W. Wang, R.-J. Qi, X.-L. Hu, *Angew. Chem.* 116 (2004) 1434-1438.
- [41] J. Zhu, M. Chen, N. Yerra, N. Haldolaarachchige, S. Pallavkar, Z. Luo, T.C. Ho, J. Hopper, D.P. Young, S. Wei, Z. Guo, *Nanoscale* 5 (2013) 1825-1830.
- [42] A.C. Metaxas, R.J. Meredith (Eds.), *Power Engineering Series* 41983.
- [43] Z. Hashisho, M. Rood, L. Botich, *Environ. Sci. Technol.* 39 (2005) 6851-6859.
- [44] I. Plazl, G. Pipus, T. Koloini, *AIChE J.* 43 (1997) 754-760.
- [45] A. Louty (Ed.), *Wiley-VCH, Weinheim Germany and Cambridge, U.K.*, 2002.
- [46] J.A. Gerbec, D. Magana, A. Washington, G.F. Strouse, *J. Am. Chem. Soc.* 127 (2005) 15791-15800.
- [47] W.X. Chen, J.Y. Lee, Z. Liu, *Chem. Commun.* (2002) 2588-2589.
- [48] P. Raveendran, J. Fu, S.L. Wallen, *Green Chem.* 8 (2006) 34-38.
- [49] H. Gu, D. Ding, P. Sameer, J. Guo, N. Yerra, Y. Huang, Z. Luo, T.C. Ho, N. Haldolaarachchige, D.P. Young, A. Kasanov, Z. Guo, S. Wei, *ECS Solid State Lett.* 3 (2013) M65-M68.
- [50] J. Zhu, M. Chen, H. Qu, H. Wei, J. Guo, Z. Luo, N. Haldolaarachchige, D.P. Young, S. Wei, Z. Guo, *J. Mater. Chem. C* 2 (2014) 715-722.
- [51] J. Zhu, H. Gu, J. Guo, M. Chen, H. Wei, Z. Luo, H.A. Colorado, N. Yerra, D. Ding, T.C. Ho, N. Haldolaarachchige, J. Hopper, D.P. Young, S. Wei, *J. Mater. Chem. A* 2 (2014) 2256-2265.
- [52] A. Burke, *J. Power Sources* 91 (2000) 37-50.
- [53] J. Zhu, S. Pallavkar, M. Chen, N. Yerra, Z. Luo, H.A. Colorado, H. Lin, N. Haldolaarachchige, A. Khasanov, T.C. Ho, D.P. Young, S. Wei, Z. Guo, *Chem. Commun.* 49 (2013) 258-260.
- [54] C. Chakkaravarthy, P. Periasamy, S. Jegannathan, K.I. Vasu, *J. Power Sources* 35 (1991) 21-35.
- [55] J. Urbaniak, J. Skowroński, B. Olejnik, *J. Solid State Electrochem.* 14 (2010) 1629-1635.
- [56] W. Xing, F. Li, Z.-f. Yan, G.Q. Lu, *J. Power Sources* 134 (2004) 324-330.
- [57] L. Cao, F. Xu, Y.Y. Liang, H.L. Li, *Adv. Mater.* 16 (2004) 1853-1857.

- [58] C. Lin, J.A. Ritter, B.N. Popov, *J. Electrochem. Soc.* 145 (1998) 4097-4103.
- [59] R.A. Tacke, L.J.J. Janssen, *J. Appl. Electrochem.* 25 (1995) 1-5.
- [60] T.Z. Fahidy, *J. Appl. Electrochem.* 13 (1983) 553-563.
- [61] R.J. Moreau (Ed.), *Magnetohydrodynamics*, Kluwer Academic Publishers, Norwell, MA, USA, 1990.
- [62] A. Chiba, K. Ogura, T. Ogawa, T. Yamashita, *Chem. Abstr.* 111 (1989) 183087.
- [63] T. Yamashita, A. Chiba, *Chem. Abstr.* 111 (1989) 183086.
- [64] L. Zhang, G. Shi, *J. Phys. Chem. C* 115 (2011) 17206-17212.
- [65] J. Zhu, S. Wei, N. Haldolaarachchige, J. He, D.P. Young, Z. Guo, *Nanoscale* 4 (2012) 152-156.
- [66] J. Bai, R. Cheng, F. Xiu, L. Liao, M. Wang, A. Shailos, K.L. Wang, Y. Huang, X. Duan, *Nat. Nanotechnol.* 5 (2010) 655-659.
- [67] J. Hu, T.F. Rosenbaum, *Nat. Mater.* 7 (2008) 697-700.
- [68] J. Zang, X. Li, *J. Mater. Chem.* 21 (2011) 10965-10969.
- [69] G. Yu, L. Hu, N. Liu, H. Wang, M. Vosgueritchian, Y. Yang, Y. Cui, Z. Bao, *Nano Lett.* 11 (2011) 4438-4442.
- [70] D. Zhang, X. Zhang, Y. Chen, P. Yu, C. Wang, Y. Ma, *J. Power Sources* 196 (2011) 5990-5996.
- [71] P. Simon, Y. Gogotsi, *Nat. Mater.* 7 (2008) 845-854.
- [72] M.B. Sassin, A.N. Mansour, K.A. Pettigrew, D.R. Rolison, J.W. Long, *ACS Nano* 4 (2010) 4505-4514.
- [73] T.-Y. Wei, C.-H. Chen, H.-C. Chien, S.-Y. Lu, C.-C. Hu, *Adv. Mater.* 22 (2010) 347-351.



Dr. Jiahua Zhu received his Ph.D. and M.S. degrees both in Chemical Engineering from Lamar University (2013) and Nanjing University of Technology (2009), respectively. He is currently an assistant professor in Chemical and Biomolecular Engineering Department at The University of Akron. His research interests involve new synthetic routes to multifunctional polymer- and carbon-based nanocomposites with advanced

applications in environmental remediation, energy storage and conversion, and micro-electronic device fabrication. He was awarded the Chinese Government Award for Outstanding Self-Financed Students Abroad in 2012 and SPE Thermoplastic Elastomers Special Interest Group Scholarship in 2013.



Dr. Minjiao Chen received Ph.D. degree in Chemistry from The Hong Kong University of Science and Technology (2012) and B.S. degree in applied chemistry from Yangzhou University (2006). Her research interests are biochemistry including bioorganic chemistry, protein chemistry, enzymology and advanced bio-applications of multifunctional nanocomposites.



Miss Huige Wei, currently a Ph.D. student in Dan F. Smith Department of Chemical Engineering at Lamar University supervised by Prof. Zhanhu Guo, obtained both her M.S. (2011) and B.E. (2009) degrees from the Department of Chemical Engineering and Technology at Harbin Institute of Technology, Harbin, China. Her research interests mainly focus on polymer based nanocomposites for electrochromic, energy storage, and anticorrosion applications.



spun multifunctional polymer nanocomposites.

Narendranath Yerra is currently a doctoral student in Dan F. Smith Department of Chemical Engineering at Lamar University. He also received his master's in Chemical Plant Design and bachelor's in chemical engineering from the National Institute of Technology (2009) and Acharya Nagarjuna University (2007), respectively. His research interests are in microwave synthesized magnetic carbon nanocomposites and electro-



Dr. Neel Haldolaarachchige is currently a postdoctoral research associate at Princeton University. He received his Ph.D. in Physics from Louisiana State University (2012), M.Sc. in Condensed Matter Physics from Norwegian University of Science & Technology (NTNU), Norway (2008) and B.Sc. in Physics from University of Peradeniya, Sri Lanka (2002). His research interest is within experimental condensed matter physics and material science broadly defined as strongly correlated electronic systems. Particularly he is studying correlations between chemical and electronic structures with physical properties of novel electronic, magnetic, and superconducting systems. His specialties are material synthesis, crystal growth, and structural and physical properties characterization.



Dr. Zhiping Luo is an Associate Professor of Physics and Materials Science at Fayetteville State University, North Carolina. He received Ph.D. from Chinese Aeronautical Establishment in 1994, followed with post-doc research at Okayama University of Science, Japan. From 1998-2001, he worked at Argonne National Laboratory as a Visiting Scholar, with a promotion to Assistant Scientist; and from 2001-2012, at Texas A&M University as a Research Scientist. His research focuses on the nanomaterials for energy-related applications, including high-sensitivity radiation detections.



Dr. Young received his Ph.D. in 1998 in experimental condensed matter physics at the National High Magnetic Field Laboratory at Florida State University. He then studied novel materials in the Chemistry Department at Princeton University before joining the faculty in the Department of Physics and Astronomy at Louisiana State University in 2000, where he currently holds the position of Professor of physics. Dr. Young's research focuses on the synthesis and characterization of strongly correlated electron materials, including: low-density carrier magnetic systems, superconductivity, and thermoelectrics. A variety of techniques are employed to make high quality polycrystalline and single crystal samples, and then magnetic, electronic, and thermal properties are measured as a function of temperature and magnetic field.



Dr. Thomas Ho, a professor in the Dan F. Smith Department of Chemical Engineering at Lamar University, obtained both his M.S and Ph.D. degrees in Chemical Engineering from Kansas State University in 1978 and 1982, respectively, and his B.S degree in Chemical Engineering from National Taiwan University in 1973. He is currently the Chair of the Department and the Director of two research centers at Lamar University funded by the state of Texas, namely, the Texas Air Research Center and the Texas Hazardous Waste Research Center. His current research focuses on the development of microwave technology for environmental remediation applications.



Dr. Suying Wei, currently an Assistant Professor in the Department of Chemistry and Biochemistry at Lamar University, obtained a chemistry Ph.D. degree from Louisiana State University (2006), a M.S. in applied chemistry from Beijing University of Chemical Technology (2000) and B.S. in chemical engineering from Shandong University of Science and Technology (1996). Her research interests are in multifunctional composites especially those towards biomedical applications. Her expertise is in

analytical, materials and surface chemistry. She was awarded NSF summer institute fellowship, Pfizer graduate fellowship and Robinson award for excellent research in analytical science during previous professional development.



Dr. Zhanhu Guo, currently an Associate Professor in Dan F. Smith Department of Chemical Engineering at Lamar University, obtained a Chemical Engineering Ph.D. degree from Louisiana State University (2005) and received three-year (2005-2008) postdoctoral training in Mechanical and Aerospace Engineering Department in University of California Los Angeles. Dr. Guo directs the Integrated Composites Laboratory and Chairs the Composite Division of American Institute of Chemical Engineers (AIChE, 2010-2011). Currently, Dr. Guo's research team focuses on fundamental science of light-weight nanocomposites especially with polymer and carbon as the hosting matrix for Energy and Sustainability applications.